Chemical Science

ROYAL SOCIETY OF CHEMISTRY

EDGE ARTICLE

View Article Online
View Journal | View Issue

Cite this: *Chem. Sci.*, 2024, **15**, 3920

All publication charges for this article have been paid for by the Royal Society of Chemistry

Received 20th November 2023
Accepted 9th February 2024

DOI: 10.1039/d3sc06191d

rsc.li/chemical-science

Multi-site isomerization of synergistically regulated stimuli-responsive AIE materials toward multi-level decryption†

Weiren Zhong,‡[ab] Jianyu Zhang,‡[c] Yuting Lin,[a] Shouji Li,[a] Yalan Yang,[a] Wen-Jin Wang,[d] Chuanling Si,*[e] Fritz E. Kühn,[f] Zheng Zhao,[d] Xu-Min Cai*[ab] and Ben Zhong Tang*[cd]

Stimuli-responsive aggregation-induced emission (AIE) materials are highly sensitive and rapidly responsive to external signals, making them ideal solid materials for anti-counterfeiting encryption. However, the limited conformational and packing variations resulting from regio-isomerization with a single substituent restricts the stimuli-responsive behavior of these materials. In this work, several AIE-active regio-structural isomers based on the salicylaldehyde Schiff base scaffold have been straightforwardly obtained through multiple substitutions with bromide and triphenylamine moieties. Solvent-effect experiments demonstrate their different orders of charge-transfer and excited-state intramolecular proton transfer upon photoexcitation, indicating the regulation of excited-state processes *via* multi-site isomerization. These isomers also demonstrate mechanochromism and acidichromism, allowing for adjustable stimuli-responsive effects. As a demonstration, *p*-Br-TPA with both mechanochromism and acidichromism can be synergistically utilized for multi-level decryption. This study successfully regulates the evolution of excited states through multi-site isomerization, offering a general approach for achieving tunable stimuli-responsive properties in AIE-active salicylaldehyde Schiff bases toward multi-level decryption.

Introduction

Stimuli-responsive optical materials can be viewed as materials that produce corresponding light signals in the presence of external stimuli such as light,[1–6] mechanical force,[7–9] pH changes,[10–12] ions,[13–19] *etc.* Due to their advantages of high sensitivity, fast response, and real-time visualization of light signals, the development of "intelligent" stimuli-responsive optical materials has attracted significant interest.[20–22] For stability and practical applications, stimuli-responsive materials are usually utilized in the solid state, where the structure as a whole may play a decisive role for the observed properties, not primarily the individual molecules.[23–25] However, traditional organic luminescent molecules with planar conformation exhibit aggregation-caused quenching effects in the solid state, affecting the optical performance of the materials.[26] In contrast, aggregation-induced emission (AIE) represents the opposite behavior: luminogens with AIE effect (AIEgens) are non-emissive in the isolated state but can emit bright light in the aggregate state.[27–29] Accordingly, AIEgens are preferable for developing "intelligent" stimuli-responsive optical materials, promoting the continuous exploration of AIE-based materials during the past two decades.[16,30–32]

Due to great structural diversity, molecular isomers exhibit a variety of photophysical properties and stimuli-responsive characteristics.[33,34] The construction of isomers often involves modifying the same functional group at different positions on the molecular scaffold.[35–38] For instance, introducing the same group (*e.g.*, –Br, –CO_2Me, and –COOH) in *ortho*, *meta*, or *para* position of a benzene ring results in molecules with different properties of mechanochromic luminescence (MCL), room-temperature phosphorescence, and pH responsiveness, respectively (Fig. 1a).[39–41] However, in these molecular scaffolds only a single functional group is modified, resulting in limited structural and property

[a]*Jiangsu Co-Innovation Center of Efficient Processing and Utilization of Forest Resources, College of Chemical Engineering, Nanjing Forestry University, Nanjing 210037, China. E-mail: xumin.cai@njfu.edu.cn*

[b]*Guangdong Provincial Key Laboratory of Luminescence from Molecular Aggregates, Guangzhou 510640, China*

[c]*Department of Chemistry, Hong Kong Branch of Chinese National Engineering Research Center for Tissue Restoration and Reconstruction, The Hong Kong University of Science and Technology, Hongkong 999077, China*

[d]*School of Science and Engineering, Shenzhen Institute of Aggregate Science and Technology, The Chinese University of Hong Kong, Shenzhen (CUHK-Shenzhen), Shenzhen 518172, China. E-mail: tangbenz@cuhk.edu.cn*

[e]*State Key Laboratory of Biobased Fiber Manufacturing Technology, Tianjin Key Laboratory of Pulp and Paper, Tianjin University of Science and Technology, Tianjin 300457, China. E-mail: sichli@tust.edu.cn*

[f]*Department of Chemistry & Catalysis Research Center, Molecular Catalysis, School of Natural Sciences, Technische Universität München, München D-85747, Germany*

† Electronic supplementary information (ESI) available. CCDC 2252820 and 2293108. For ESI and crystallographic data in CIF or other electronic format see DOI: https://doi.org/10.1039/d3sc06191d

‡ W. Zhong and J. Zhang contributed equally to this work.

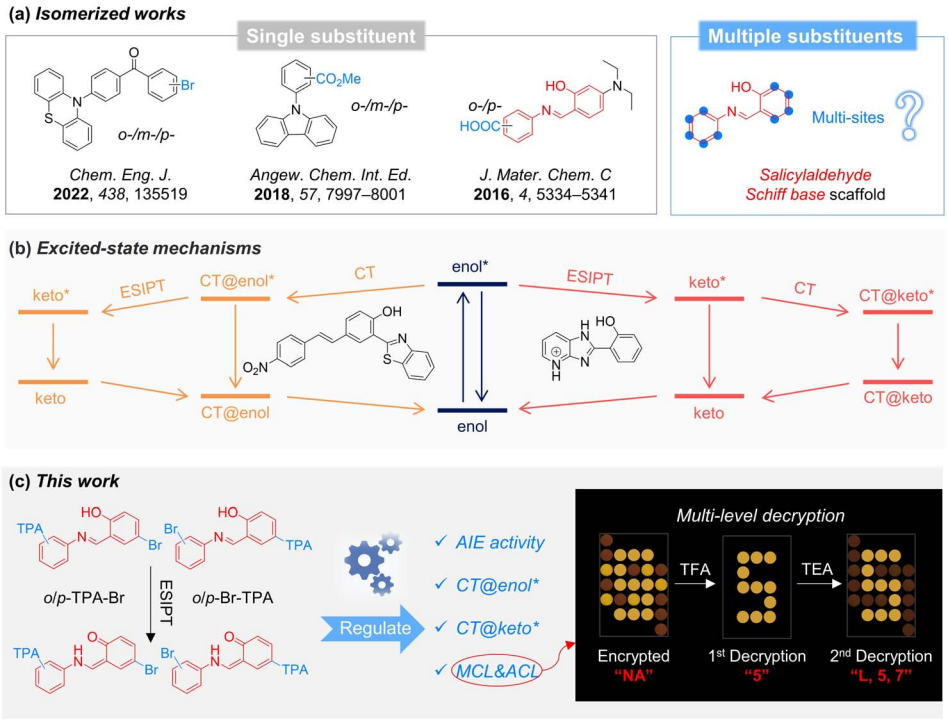

Fig. 1 (a) Structures of conventional single-substituent molecules (I–III) and the salicylaldehyde Schiff base scaffold with multi-site substitutions (IV). (b) The different paths and order of excited-state processes of CT and ESIPT. (c) Molecular design and properties of multi-substituted salicylaldehyde Schiff bases in this work. CT: charge transfer, ESIPT: excited-state intramolecular proton transfer, MCL: mechanochromic luminescence, ACL: acidichromic luminescence.

variations. As shown in the marginal molecule of Fig. 1a, the salicylaldehyde Schiff base scaffold with two benzene rings shows several available substitution sites, rendering it a versatile and easily diversifiable framework structure. This scaffold is prone to isomerization and possesses imine bonds, which endows it with various stimuli-responsive properties such as thermochromism, photochromism, and acidochromism.[42–44] Hence, various isomers can be generated by utilizing multiple functional groups, resulting in a variety of photophysical and enhanced stimulus-responsive properties.[45] Besides, the imine and hydroxyl groups in the salicylaldehyde Schiff base scaffold enable excited-state intramolecular proton transfer (ESIPT),[46,47] where the enol form can transform into the keto structure upon photoexcitation. On the other hand, propeller triphenylamine (TPA), as a star fragment for AIEgens, is commonly used to construct stimuli-responsive systems.[27,48] Additionally, its strong electron-donating ability endows it with donor–acceptor (D–A) abilities and allows intramolecular charge transfer (ICT) processes.[49,50] Therefore, incorporating TPA groups into the salicylaldehyde Schiff base scaffold may help to achieve multiple photophysical processes such as AIE, ESIPT, and ICT simultaneously. Interestingly, previous works report that the CT process occurs in the enol form (CT@enol*) before ESIPT and in the keto form (CT@keto*) after ESIPT within different molecular systems, respectively (Fig. 1b).[51,52] However, the mechanism behind the order of CT and ESIPT is still poorly understood, and it is still challenging to realize the regulation of these two processes within the same molecular skeleton.[53] Therefore, it is significant to construct novel AIE-based stimuli-responsive materials by regulating the photophysical mechanisms and responsive properties of salicylaldehyde Schiff base through multi-site isomerization strategies.

In this work, various salicylaldehyde Schiff base isomers (*o*-TPA-Br, *p*-TPA-Br, *o*-Br-TPA, and *p*-Br-TPA) were synthesized by modifying different substituent positions of TPA and bromine units. All of them are non-emissive in diluted solution but highly emissive in the aggregate state, suggesting the typical AIE effect. In addition, they exhibit different orders of ESIPT and ICT in the excited state upon photoexcitation, indicating the manipulation of excited-state behavior through the multi-substituent strategy. Interestingly, *p*-TPA-Br exhibits both stimuli-responsive MCL and acidichromic luminescent (ACL) properties, which has been successfully utilized for multi-level decryption (Fig. 1c). This work constructs several salicylaldehyde Schiff base isomers with multiple properties and provides a general strategy to manipulate stimuli-responsive materials by multi-site isomerization toward multi-level decryption.

Results and discussion

Synthesis and characterization

The synthetic pathways to *p*-TPA-Br, *o*-Br-TPA, and *p*-Br-TPA are shown in Scheme S1.† The structures and purity of these compounds are confirmed by ^{1}H NMR, ^{13}C NMR, HRMS, and single-crystal X-ray diffraction techniques (Fig. S1–S9 and Table S1†).

ESIPT-AIE properties

The absorption properties of the above-mentioned compounds were first measured and compared (Fig. S10†). All of them show their maximum absorption peaks at around 380 nm. *o*-TPA-Br is a typical AIE molecule, according to our previous work.[54] Then, the PL properties of *p*-TPA-Br, *o*-Br-TPA, and *p*-Br-TPA were investigated in acetonitrile (ACN)/water mixtures (Fig. 2). As shown in their fluorescent photographs, they are nonemissive in pure ACN solutions but gradually become emissive with increasing water fractions (f_w), suggesting a typical AIE feature (Fig. 2b). Interestingly, the PL spectra show different luminescence features. Compared to the maximum absorption wavelength at 375 nm, *p*-TPA-Br exhibits an emission peak at 555 nm with a significant Stokes shift, belonging to the emission of the keto form (Fig. 2c). However, *o*-Br-TPA and *p*-Br-TPA show dual-peak emission (Fig. 2d and e). The short-wavelength peak at about 400 nm is dominant in *o*-Br-TPA, while the long-wavelength peak at 600 nm becomes dominant in *p*-Br-TPA. The former peak is ascribed to the emission from the enol form, and the latter corresponds to the keto form. The above-described results indicate different ESIPT properties of these compounds upon photoexcitation. In addition, PL spectra and the relative emission intensity (α_{AIE}) curves also demonstrate their AIE properties as evidenced by the sharply increased emission intensity from the keto form when f_w rises from 60% to 90% (Fig. 2f). Moreover, concentration-dependent, viscosity-dependent PL spectra and low-temperature photographs prove the mechanism of restriction of intramolecular motion (RIM) for the AIE property (Fig. S11–13†). Therefore, the obtained results clearly suggest that these four salicylaldehyde Schiff-based isomers possess varied ESIPT and AIE properties.

The different excited-state processes

According to the design strategy, TPA is an intrinsic electron-donating group, and the salicylaldehyde Schiff base part is a weak electron-withdrawing group, suggesting the D–A structure and the ICT properties of these isomers. The absorption spectra show that their absorption maxima are almost identical but have different absorbances (Fig. S14†). However, these isomers exhibit different PL properties in different polar solvents (Fig. S15†). Taking *o*-TPA-Br as an example, two emission peaks from the enol and keto forms are observed in different solvents (Fig. S15a†). The emission wavelength of the enol-form peak undergoes significant changes with varying solvent polarity, while that of the keto form remains the same. However, other molecules exhibit the opposite changes in properties of the enol and the keto form peak (Fig. S15b–d†). Hence, further analysis is performed concerning the polarity dependence of their luminescent profiles. As shown in Fig. 3a, further comparison of the enol-form emission of *o*-TPA-Br reveals that the peak gradually redshifts with increasing solvent polarity. The emission wavelength in DMSO redshifts by 20 nm compared to that in Et_2O, indicating that *o*-TPA-Br is more prone to undergo CT in the enol state, followed by an ESIPT process.[55] On the other hand, the other three isomers of *p*-TPA-Br, *o*-Br-TPA, and *p*-Br-TPA exhibit a noticeable redshift

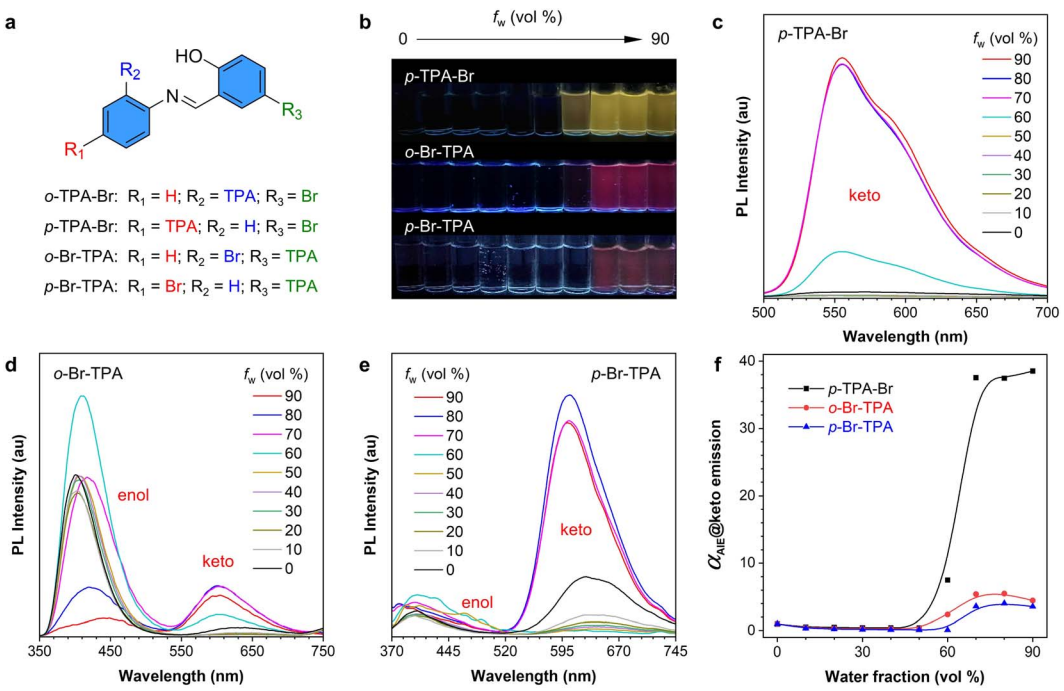

Fig. 2 (a) Chemical structures of the four isomers. (b) The fluorescence photographs of the four isomers in ACN/H_2O mixtures with different water fractions (f_w) at room temperature, taken under 365 nm UV irradiation. Concentration: 20 μM. (c–e) PL spectra of (c) *p*-TPA-Br, (d) *o*-Br-TPA, and (e) *p*-Br-TPA in ACN/H_2O with different f_w. Concentration: 20 μM. λ_{ex}: 375 nm for *p*-TPA-Br, 326 nm for *o*-Br-TPA, and 320 nm for *p*-Br-TPA. (f) The plots of the relative emission intensity ($\alpha_{AIE} = I/I_0$) *versus* the different f_w of the four isomers.

(32 nm, 52 nm, and 36 nm, respectively) of the keto-form emission with increasing solvent polarity (Fig. 3b–d). This suggests that they first undergo an ESIPT process in the excited state, followed by the CT process in the keto form.[52,56,57] Therefore, these isomers exhibit different orders of the ESIPT and CT processes, namely the CT effect in the enol (CT@enol*) and keto (CT@keto*) form respectively in the excited state upon photoexcitation. From the molecular structures (Fig. S16†), we can infer that the small adjacent substituents (bromine and hydrogen) to the aniline moiety of *p*-TPA-Br, *o*-Br-TPA, and *p*-Br-TPA could cause the absence of steric hindrance around the six-membered ring structure in the excited state, which allows for a more accessible occurrence of the ESIPT, followed by CT process. While the large TPA group adjacent to the aniline moiety of *o*-TPA-Br introduces certain steric hindrance effects on the six-membered ring.[58] In other words, the excited-state behaviors of these isomers are regulated by modulating the position of multi-substituents in the salicylaldehyde Schiff base scaffold.

Mechanochromic luminescence properties

MCL is closely related to the molecular packing and intermolecular interactions in the aggregate state. The multi-site-based isomerization strategy provides a general method to construct molecules with different aggregate-state structures, which may endow them with different MCL properties. Therefore, the mechano-responsive behaviors of these salicylaldehyde Schiff base isomers were investigated. According to the PL spectra (Fig. 4a), *p*-Br-TPA exhibits no fluorescence in the pristine (crystalline) state. However, it shows a distinct emission peak in the range of 600–650 nm after grinding, indicating a red fluorescence emission. Similarly, the pristine *p*-TPA-Br exhibits a weak emission peak at 570 nm, which is enhanced and shifts to 560 nm after grinding (Fig. 4b). As shown in Fig. 4c, the PXRD reveals that pristine *p*-Br-TPA and *p*-TPA-Br exhibit sharp diffraction peaks, indicating an ordered arrangement of their single crystals. After grinding, the decrease in diffraction peak intensity suggests an amorphous state of these samples with destroyed molecular stacking. These results indicate typical MCL properties of *p*-Br-TPA and *p*-TPA-Br. In contrast, *o*-TPA-Br and *o*-Br-TPA do not display such properties (Fig. S17†). To further elucidate the mechanism of MCL, single crystals of *o*-Br-TPA and *p*-Br-TPA were obtained by slow precipitation in appropriate solvents (Table S1†). The single-crystal data of *o*-TPA-Br were reported previously.[54] According to the single-crystal structure, the twisting angle between the aniline moiety and the salicylaldehyde moiety of *p*-Br-TPA is 1.83°, indicating an almost planar conformation. Furthermore, the packing shows an ordered and continuous arrangement of dimers (Fig. 4d). The face-to-face distance between each dimer is measured to be 3.355 Å, smaller than the critical value of 3.5 Å for π–π stacking.[59] Therefore, the strong and continuous π–π stacking in the pristine crystal is the primary cause of fluorescence quenching.[60] In comparison, *o*-TPA-Br and *o*-Br-TPA without MCL properties exhibit no indistinct π–π stacking within their crystal arrangements (Fig. S18†). Force stimuli may not bring them with significant packing changes, explaining the deficiency of enhanced fluorescence intensity. Based on the MCL behavior of *p*-Br-TPA and *p*-TPA-Br, a force stimulus disrupts π–π stacking and reduces non-radiative dissipation, leading to enhanced fluorescence intensity (Fig. 4e). Based on these results, the multi-site isomerization strategy enables isomers to achieve MCL behavior.

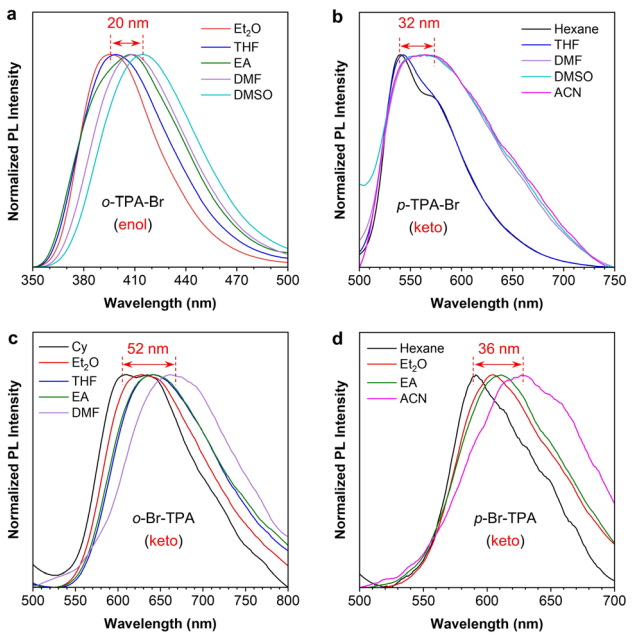

Fig. 3 Normalized PL spectra of (a) *o*-TPA-Br, (b) *p*-TPA-Br, (c) *o*-Br-TPA, and (d) *p*-Br-TPA in solvents with varying polarity. Concentration: 20 μM.

Mono-level decryption *via* acidichromic luminescence

Schiff base skeletons with an imine group always show acid/base-responsive properties and ACL effects. Therefore, the ACL effect of these four isomers was further investigated. Among them, *o*-TPA-Br, *p*-TPA-Br, and *o*-Br-TPA exhibit ACL properties, wherein their fluorescence is quenched upon acid stimulation and recovered after exposure to alkaline vapor (Fig. 5 and S19†). Since its simultaneous MCL and ACL performance, *p*-TPA-Br is selected as the model for further demonstrations. The pristine *p*-TPA-Br exhibits a prominent emission peak at 560–590 nm (Fig. 5a). After exposure to TFA vapor for 5 s, the sample becomes non-emissive. The acid stimulation causes the protonation structure, strengthening the ICT effect. Accordingly, molecules with strong ICT effects could exhibit low oscillator strength between the excited and ground states, leading to nonradiative transitions that may quench its fluorescence.[61,62] After TEA vapor fuming for 5 minutes, the emission is almost completely recovered because of deprotonation progress to the initial state. To further explore the mechanism of ACL, UV absorption and NMR tests were conducted on this isomer before and after acid treatment. As the excess equivalent of TFA is added to the ACN solution, the maximum absorption wavelength of *p*-Br-TPA gradually undergoes a redshift,

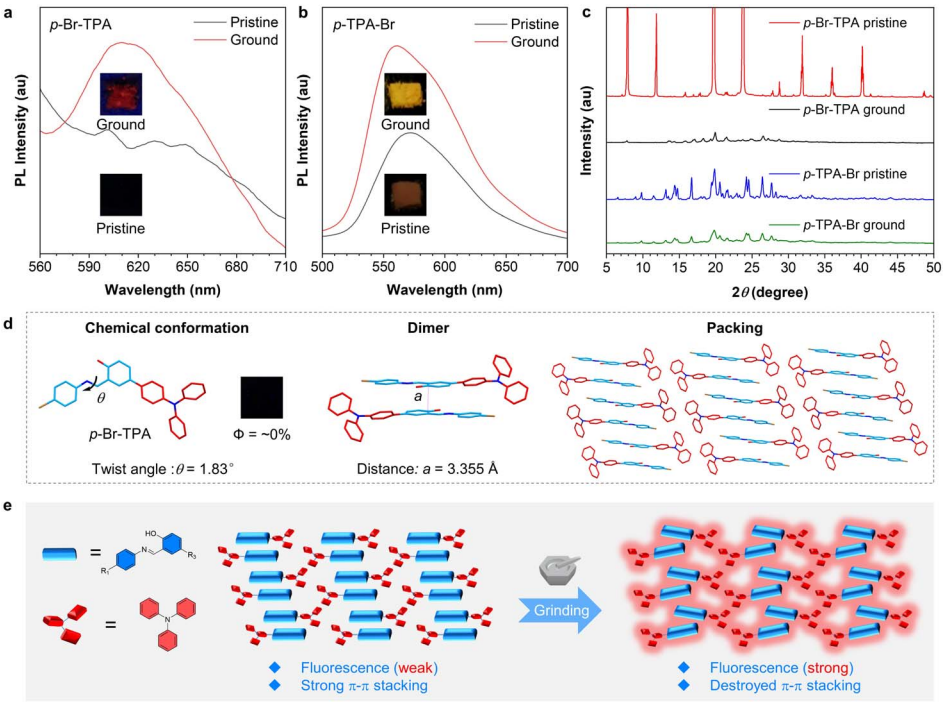

Fig. 4 (a and b) PL spectra of (a) *p*-Br-TPA and (b) *p*-TPA-Br before and after grinding. *p*-Br-TPA: $\lambda_{ex} = 443$ nm; *p*-TPA-Br: $\lambda_{ex} = 375$ nm. (c) PXRD patterns of *p*-Br-TPA and *p*-TPA-Br (pristine and ground). (d) Chemical conformation, dimer, and packing of *p*-Br-TPA. (e) Schematic illustration of the proposed fluorescence mechanism.

indicating the protonated compound (Fig. S20†).[63] As shown in Fig. 5b, the hydrogen signal of –N=CH– moves downfield upon the addition of TFA because of the altered chemical environment caused by protonation.[64] Upon the addition of TEA, the hydrogen signal moves upfield, reflecting the recovery process of deprotonation. Simultaneously, the hydrogen signals in 7.0–8.0 ppm show the same trend upon the additional TFA and TEA. The ^{1}H NMR spectra of *o*-TPA-Br and *o*-Br-TPA, as shown in Fig. S21,† exhibit similar chemical shift trends. With the help of sequential fluorescence quenching and recovery of *p*-TPA-Br

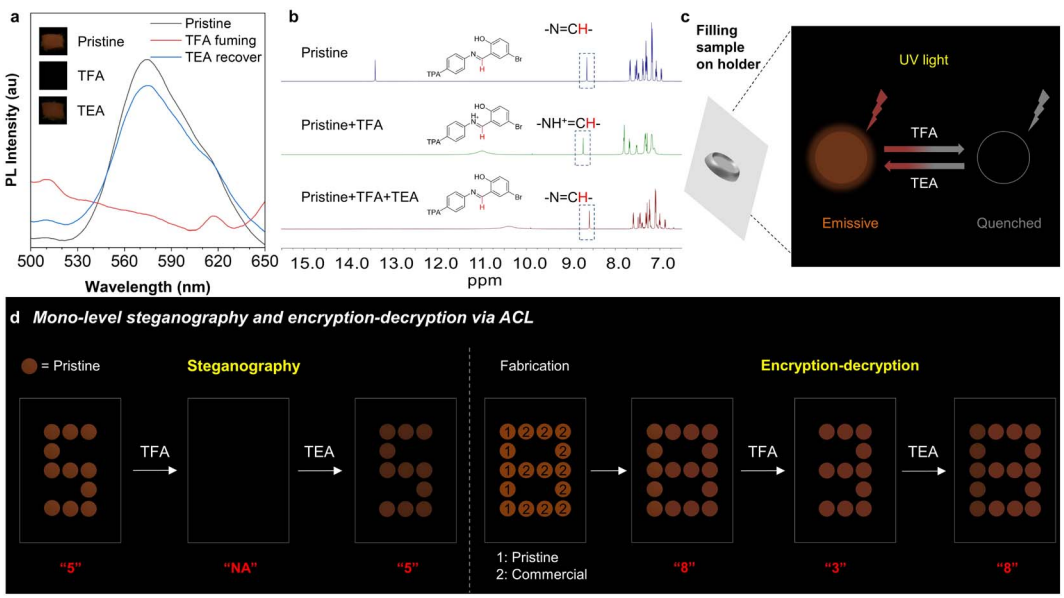

Fig. 5 (a) PL spectra of *p*-TPA-Br as solid: pristine, sample fumed with TFA, sample fumed with TEA. Inset: fluorescence photographs taken after different treatments. (b) ^{1}H NMR spectra of *p*-TPA-Br in $CDCl_3$ before and after TFA and TEA in 7.0–15.0 ppm region. (c) Schematic diagram of the sample holder with TFA and TEA responses. (d) Schematic diagram of mono-level steganography and encryption–decryption.

upon acid/base stimuli, a mono-level encryption system could be achieved through the arrangement of holders filled with solid samples (Fig. 5c). Accordingly, the number of "5" is displayed as the initial information with red emission. After exposure to TFA vapor, the number of "5" undergoes fluorescence quenching and cannot be seen anymore. The number could be displayed again after subsequent exposure to TEA, demonstrating the applicability of *p*-TPA-Br for steganography. In addition, by combining a commercial fluorescent dye with the same color, a number of "8" can be displayed. Fluorescence of a commercial fluorescent dye does not undergo ACL after exposure to acid. Therefore, only the number of "3" appears after exposure to acid vapor, achieving an encrypting effect. After subjecting the system to TEA vapor, the complete information of "8" is revealed, achieving the whole encryption–decryption procedure (Fig. 5d). These demonstrations prove that *p*-TPA-Br can serve as a functional material for simple information decryption.

Multi-level decryption *via* synergistic regulation of MCL and ACL

The mono-stimulus response can only provide simple steganography and mono-level encryption–decryption applications. Conversely, a collaborative multi-stimulus response from the same material can offer a range of information transformations and enable multi-level encryption–decryption, thereby enhancing the security of information protection. Based on the experiments described above, only *p*-TPA-Br exhibits both MCL and ACL properties. The pristine *p*-TPA-Br exhibits weak fluorescence, which could be quenched and restored upon acid and base vapor treatment. Besides, it produces strong yellow fluorescence after grinding, which can be converted to the initial state with weak fluorescence after base vapor treatment (Fig. 6a and S22†). Such a combination of MCL and ACL responses enables a unified change in fluorescence signals. Therefore, we investigated the potential ability of *p*-TPA-Br for multi-level encryption–decryption of information. In order to obtain diversified fluorescence signal information, an additional commercial fluorescent dye with the same color but without stimuli-responsive properties was also utilized. As shown in Fig. 6b(I), different circular slots were filled with the pristine *p*-TPA-Br, ground *p*-TPA-Br, or commercial fluorescent dye. Different fluorescence from these compounds results in a chaotic signal that cannot provide effective information. After acid-vapor treatment, both pristine and ground samples are affected, resulting in fluorescence quenching. Based on the fluorescence signal of the commercial dye, the information as the number "3" can be decrypted. Then, after undergoing base-vapor treatment, the fluorescence of two-state *p*-TPA-Br is restored and unified, enabling the second round decryption with combined information of letter and number as "E3", achieving multi-level information decryption. Following the same principle, more complex alphanumeric data such as "5" and "L,5,7" can be encrypted and decrypted. Furthermore, to achieve diversified encryption–decryption of information, we also explored its potential for image encryption–decryption

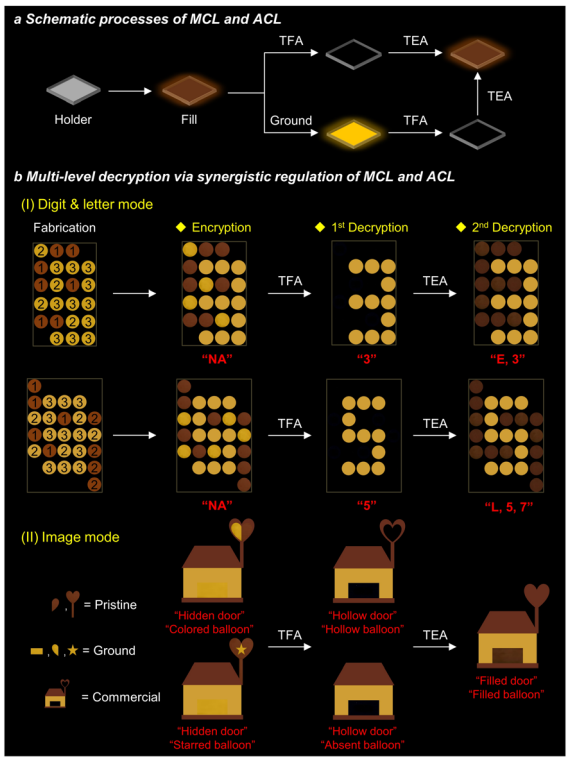

Fig. 6 (a) Schematic progress of MCL and ACL of *p*-TPA-Br. (b) Multi-level decryption *via* synergistic regulation of MCL and ACL of *p*-TPA-Br (digit 1: pristine; digit 2: ground; digit 3: commercial).

(Fig. 6b(II)). In this case, the combination of pristine and ground *p*-TPA-Br and the commercial dye shows an image of a house with balloons. The original image features a hidden door and multi-colored balloons. After acid treatment, the door appears, and the balloons become hollow or disappear, respectively, representing the first decryption of the image. After base treatment, the door is filled, and the balloons appear with consistent colors, representing the second decryption of the image. This example again demonstrates that *p*-TPA-Br can achieve multi-level encryption–decryption in the image mode. Thereby, by synergistically controlling the MCL and ACL properties of *p*-TPA-Br, diversified information can be encrypted and decrypted at several levels, realizing encryption–decryption and enhancing information security.

Conclusions

In this work, four AIE-active isomers (*o*-TPA-Br, *p*-TPA-Br, *o*-Br-TPA, and *p*-Br-TPA) were synthesized by utilizing two substituents, namely TPA and Br on a multi-site of a salicylaldehyde Schiff base scaffold. With the help of the Schiff base skeleton and a TPA unit as the electron donor, they show typical ESIPT and ICT properties. Interestingly, the order of ESIPT and ICT in the excited state could be manipulated *via* the multi-substituent strategy. *o*-TPA-Br undergoes the ICT process followed by the ESIPT, as evidenced by the redshifted emission from the enol form. In contrast, *p*-TPA-Br, *o*-Br-TPA, and *p*-Br-TPA show ESIPT followed by the ICT emission from the keto-form conformation. On the

other hand, stimuli-responsive properties of these isomers can also be achieved. *p*-TPA-Br and *p*-Br-TPA show force-enhanced fluorescence, which can be attributed to the disruption of π–π stacking by mechanical force stimuli. More significantly, *p*-TPA-Br possesses both mechanochromism and acidichromism, which could be synergistically utilized as stimuli-responsive materials for multi-level decryption to enhance the security level of information. Therefore, the multi-site isomerization strategy reported in this work realizes a dual-regulation effect of excited-state processes and stimuli responses and provides an approach to construct novel AIE stimuli-responsive optical materials toward multi-level decryption.

Data availability

The datasets supporting this article have been uploaded as part of the ESI.†

Author contributions

Weiren Zhong: validation, formal analysis, investigation, writing – original draft. Jianyu Zhang: validation, formal analysis, investigation, writing – review & editing. Yuting Lin: investigation. Shouji Li: investigation. Yalan Yang: investigation. Wen-Jin Wang: investigation. Chuanling Si: funding acquisition, supervision, validation. Fritz E. Kühn: formal analysis, validation, writing – review & editing. Zheng Zhao: formal analysis, validation. Xu-Min Cai: conceptualization, methodology, formal analysis, resources, data curation, writing – review & editing, visualization, supervision, project administration, funding acquisition. Ben Zhong Tang: funding acquisition, supervision, validation.

Conflicts of interest

There are no conflicts to declare.

Acknowledgements

The authors were grateful to the National Natural Science Foundation of China (21601087 and 32271814), Natural Science Foundation of Jiangsu Province (BK20231296), the Open Fund of Guangdong Provincial Key Laboratory of Luminescence from Molecular Aggregates, Guangzhou 510640, China (South China University of Technology (2023B1212060003)), the Shenzhen Key Laboratory of Functional Aggregate Materials (ZDSYS20211021111400001), the Science Technology Innovation Commission of Shenzhen Municipality (KQTD20210811090142053), and the AIE Institute (**https://www.aietech.org.cn/**) for providing some AIE materials and technical assistance. J. Zhang acknowledged the support from the Research Grants Council of the Hong Kong Special Administrative Region, China (HKUST PDFS2324-6S01).

Notes and references

1 J.-L. Zhao, M.-H. Li, Y.-M. Cheng, X.-W. Zhao, Y. Xu, Z.-Y. Cao, M.-H. You and M.-J. Lin, *Coord. Chem. Rev.*, 2023, **475**, 214918.
2 N. Bar and P. Chowdhury, *ACS Appl. Electron. Mater.*, 2022, **4**, 3749–3771.
3 X.-M. Cai, Y. Lin, Y. Li, X. Chen, Z. Wang, X. Zhao, S. Huang, Z. Zhao and B. Z. Tang, *Nat. Commun.*, 2021, **12**, 1773.
4 Q. Liu, J. Tian, Y. Tian, Q. Sun, D. Sun, F. Wang, H. Xu, G. Ying, J. Wang, A. K. Yetisen and N. Jiang, *ACS Nano*, 2021, **15**, 515–525.
5 P. Zhou and K. Han, *Aggregate*, 2022, **3**, e160.
6 J. Zhang, H. Shen, X. Liu, X. Yang, S. L. Broman, H. Wang, Q. Li, J. W. Y. Lam, H. Zhang, M. Cacciarini, M. B. Nielsen and B. Z. Tang, *Angew. Chem., Int. Ed.*, 2022, **61**, e202208460.
7 F. Khan, A. Ekbote, G. Singh and R. Misra, *J. Mater. Chem. C*, 2022, **10**, 5024–5064.
8 L. Wang, L. Liu, B. Xu and W. Tian, *Chem. Res. Chin. Univ.*, 2021, **37**, 100–109.
9 X.-M. Cai, Z. Tang, X. Chen, Y. Lin, X. Zhang and S. Huang, *Dyes Pigm.*, 2022, **204**, 110454.
10 Z. Li, Z. Yang, Y. Zhang, B. Yang and Y. W. Yang, *Angew. Chem., Int. Ed.*, 2022, **61**, e202206144.
11 Y. Xiong, W. Zhong, X. Zhang, Y. Lin, Z. Tang, S. Li and X.-M. Cai, *Dyes Pigm.*, 2023, **218**, 111475.
12 J. Zhang, Y. Tu, H. Shen, J. W. Y. Lam, J. Sun, H. Zhang and B. Z. Tang, *Nat. Commun.*, 2023, **14**, 3772.
13 X. Yuan, M. Li, T. Meng, J. Mack, R. Soy, T. Nyokong, W. Zhu, H. Xu and X. Liang, *Dyes Pigm.*, 2018, **158**, 188–194.
14 L. Sun, X. Wang, J. Shi, S. Yang and L. Xu, *Spectrochim. Acta, Part A*, 2021, **249**, 119303.
15 S. Yang, L. Sun, Z. Song and L. Xu, *Front. Bioeng. Biotechnol.*, 2021, **9**, 642138.
16 S. Wu, Y. Yang, Y. Cheng, S. Wang, Z. Zhou, P. Zhang, X. Zhu, B. Wang, H. Zhang, S. Xie, Z. Zeng and B. Z. Tang, *Aggregate*, 2022, **4**, e287.
17 L. Sun, L. Chen, Z. Yang, X. Sun, D. Jin, Y. Qiu and W. Gu, *J. Food Compos. Anal.*, 2023, **120**, 105316.
18 L. Sun, Z. Wang, L. Chen, X. Sun, Z. Yang and W. Gu, *Analyst*, 2023, **148**, 1867–1876.
19 L. Chen, B. Lv, Z. Wang, L. Sun, X. Sun, J. Li and W. Gu, *Dyes Pigm.*, 2023, **220**, 111680.
20 J. Zhang, B. He, Y. Hu, P. Alam, H. Zhang, J. W. Y. Lam and B. Z. Tang, *Adv. Mater.*, 2021, **33**, e2008071.
21 C. McDonagh, C. S. Burke and B. D. MacCraith, *Chem. Rev.*, 2008, **108**, 400–422.
22 Y. Wang, T. Xu, K. Liu, M. Zhang, X.-M. Cai and C. Si, *Aggregate*, 2023, **4**, e428.
23 Y. Wang, D. Han, X. Zhou, Z. Zhang, J. Gong, H. Li and Q. Zhang, *Chem. Eng. J.*, 2023, **456**, 141052.
24 I. Maji, S. Mahajan, A. Sriram, P. Medtiya, R. Vasave, D. K. Khatri, R. Kumar, S. B. Singh, J. Madan and P. K. Singh, *J. Controlled Release*, 2021, **337**, 646–660.
25 J. Heo, D. P. Murale, H. Y. Yoon, V. Arun, S. Choi, E. Kim, J.-S. Lee and S. Kim, *Aggregate*, 2022, **3**, e159.

26 J. Mei, Y. Hong, J. W. Y. Lam, A. Qin, Y. Tang and B. Z. Tang, *Adv. Mater.*, 2014, **26**, 5429–5479.
27 J. Mei, N. L. C. Leung, R. T. K. Kwok, J. W. Y. Lam and B. Z. Tang, *Chem. Rev.*, 2015, **115**, 11718–11940.
28 X.-M. Cai, Y. Lin, J. Zhang, Y. Li, Z. Tang, X. Zhang, Y. Jia, W. Wang, S. Huang, P. Alam, Z. Zhao and B. Z. Tang, *Natl. Sci. Rev.*, 2023, **10**, nwad233.
29 T. Guo, Y. Lin, D. Pan, X. Zhang, W. Zhu, X.-M. Cai, G. Huang, H. Wang, D. Xu, F. E. Kühn, B. Zhang and T. Zhang, *Nat. Commun.*, 2023, **14**, 6076.
30 D. Shimoyama and F. Jäkle, *Aggregate*, 2022, **3**, e149.
31 Y. Zhang, S. Xie, Z. Zeng and B. Z. Tang, *Matter*, 2020, **3**, 1862–1892.
32 P. Chowdhury, A. Banerjee, B. Saha, K. Bauri and P. De, *ACS Biomater. Sci. Eng.*, 2022, **8**, 4207–4229.
33 P. Meti, D.-J. Park and Y.-D. Gong, *Dyes Pigm.*, 2019, **168**, 357–368.
34 A. Ekbote, S. M. Mobin and R. Misra, *J. Mater. Chem. C*, 2018, **6**, 10888–10901.
35 P. Zhang, Q. Shen, Y. Zhou, F. He, B. Zhao, Z. Wang, R. Xu, Y. Xu, Z. Yang, L. Meng and D. Dang, *Chin. Chem. Lett.*, 2023, **34**, 107910.
36 M. Chen, J. Liu, F. Liu, H. Nie, J. Zeng, G. Lin, A. Qin, M. Tu, Z. He, H. H. Y. Sung, I. D. Williams, J. W. Y. Lam and B. Z. Tang, *Adv. Funct. Mater.*, 2019, **29**, 1903834.
37 G. Meng, X. Chen, X. Wang, N. Wang, T. Peng and S. Wang, *Adv. Opt. Mater.*, 2019, **7**, 1900130.
38 Y. Huo, H. Qi, S. He, J. Li, S. Song, J. Lv, Y. Liu, L. Peng, S. Ying and S. Yan, *Aggregate*, 2023, **4**, 391.
39 H. Deng, Z. Yang, G. Li, D. Ma, Z. Xie, W. Li, Z. Mao, J. Zhao, Z. Yang, Y. Zhang and Z. Chi, *Chem. Eng. J.*, 2022, **438**, 135519.
40 Y. Xiong, Z. Zhao, W. Zhao, H. Ma, Q. Peng, Z. He, X. Zhang, Y. Chen, X. He, J. W. Y. Lam and B. Z. Tang, *Angew. Chem., Int. Ed.*, 2018, **57**, 7997–8001.
41 L. Hu, Y. Duan, Z. Xu, J. Yuan, Y. Dong and T. Han, *J. Mater. Chem. C*, 2016, **4**, 5334–5341.
42 M. Avadanei, V. Cozan, S. Shova and J. A. Paixão, *Chem. Phys.*, 2014, **444**, 43–51.
43 H. Sun, S.-S. Sun, F.-F. Han, Z.-H. Ni, R. Zhang and M.-D. Li, *J. Mater. Chem. C*, 2019, **7**, 7053–7060.
44 J. Shu, T. Ni, X. Liu, B. Xu, L. Liu, W. Chu, K. Zhang and W. Jiang, *Dyes Pigm.*, 2021, **195**, 109708.
45 X.-M. Sun, J. Liu, Z.-H. Li, Y.-P. Fu, T.-T. Huang, Z.-D. Tang, B. Shi, H. Yao, T.-B. Wei and Q. Lin, *Chin. Chem. Lett.*, 2023, **34**, 107792.
46 E. Hadjoudis and I. M. Mavridis, *Chem. Soc. Rev.*, 2004, **33**, 579–588.
47 V. S. Padalkar and S. Seki, *Chem. Soc. Rev.*, 2016, **45**, 169–202.
48 W. Zhao, Z. He, Q. Peng, J. W. Y. Lam, H. Ma, Z. Qiu, Y. Chen, Z. Zhao, Z. Shuai, Y. Dong and B. Z. Tang, *Nat. Commun.*, 2018, **9**, 3044.
49 Y. Yu, H. Xing, D. Liu, M. Zhao, H. H. Sung, I. D. Williams, J. W. Y. Lam, G. Xie, Z. Zhao and B. Z. Tang, *Angew. Chem., Int. Ed.*, 2022, **61**, e202204279.
50 Z. Wang, F. Zhou, J. Wang, Z. Zhao, A. Qin, Z. Yu and B. Z. Tang, *Sci. China: Chem.*, 2017, **61**, 76–87.
51 J. Ding, L. Yu, Y. Liu, Z. Yang and Y. Zhang, *Dyes Pigm.*, 2021, **191**, 109359.
52 A. Brenlla, M. Veiga, J. L. Perez Lustres, M. C. Rios Rodriguez, F. Rodriguez-Prieto and M. Mosquera, *J. Phys. Chem. B*, 2013, **117**, 884–896.
53 A. P. Demchenko, K. C. Tang and P. T. Chou, *Chem. Soc. Rev.*, 2013, **42**, 1379–1408.
54 X.-M. Cai, W. Zhong, Z. Deng, Y. Lin, Z. Tang, X. Zhang, J. Zhang, W. Wang, S. Huang, Z. Zhao and B. Z. Tang, *Chem. Eng. J.*, 2023, **466**, 143353.
55 C.-C. Hsieh, C.-M. Jiang and P.-T. Chou, *Acc. Chem. Res.*, 2010, **43**, 1364–1374.
56 M. Das, M. Brahma and G. Krishnamoorthy, *J. Phys. Chem. B*, 2021, **125**, 2339–2350.
57 L. M. Carneiro, A. F. Keppler, F. F. Ferreira, P. Homem-de-Mello and F. H. Bartoloni, *J. Phys. Chem. B*, 2022, **126**, 7373–7384.
58 X. M. Cai, S. Li, W. J. Wang, Y. Lin, W. Zhong, Y. Yang, F. E. Kühn, Y. Li, Z. Zhao and B. Z. Tang, *Adv. Sci.*, 2023, **10**, 2307078.
59 Y. Gu, Z. Zhao, H. Su, P. Zhang, J. Liu, G. Niu, S. Li, Z. Wang, R. T. K. Kwok, X.-L. Ni, J. Sun, A. Qin, J. W. Y. Lam and B. Z. Tang, *Chem. Sci.*, 2018, **9**, 6497–6502.
60 P. Alam, N. L. C. Leung, Y. Cheng, H. Zhang, J. Liu, W. Wu, R. T. K. Kwok, J. W. Y. Lam, H. H. Y. Sung, I. D. Williams and B. Z. Tang, *Angew. Chem., Int. Ed.*, 2019, **58**, 4536–4540.
61 H. Xiao, K. Ye, C. Liu, X. Yang, J. Sun and R. Lu, *Dyes Pigm.*, 2023, **215**, 111241.
62 F. Kournoutas, I. K. Kalis, M. Fecková, S. Achelle and M. Fakis, *J. Photochem. Photobiol. A*, 2020, **391**, 112398.
63 L. Yu, Q.-Y. Zhu, Y. Zhang, Z.-X. Lei, G.-Y. Niu and J. Dai, *J. Phys. Chem. A*, 2008, **112**, 13672–13678.
64 P. Xue, P. Chen, J. Jia, Q. Xu, J. Sun, B. Yao, Z. Zhang and R. Lu, *Chem. Commun.*, 2014, **50**, 2569–2571.